The bone morphogenetic protein axis is a positive regulator of skeletal muscle mass

Catherine E. Winbanks,[1] Justin L. Chen,[1,2,8] Hongwei Qian,[1] Yingying Liu,[1] Bianca C. Bernardo,[1] Claudia Beyer,[1] Kevin I. Watt,[1] Rachel E. Thomson,[1] Timothy Connor,[3] Bradley J. Turner,[4] Julie R. McMullen,[1] Lars Larsson,[6] Sean L. McGee,[3] Craig A. Harrison,[2,8] and Paul Gregorevic[1,5,7,8]

[1]Division of Cell Signaling and Metabolism, Baker IDI Heart and Diabetes Institute, Melbourne 3004, Australia
[2]Prince Henry's Institute of Medical Research, Melbourne 3168, Australia
[3]School of Medicine, Deakin University, Geelong 3217, Australia
[4]Florey Institute of Neuroscience and Mental Health and [5]Department of Physiology, The University of Melbourne, Melbourne 3010, Australia
[6]Department of Neuroscience, Uppsala University Hospital, Uppsala 75105, Sweden
[7]Department of Neurology, The University of Washington School of Medicine, Seattle, WA 98195
[8]Department of Biochemistry and Molecular Biology, Monash University, Melbourne 3800, Australia

Although the canonical transforming growth factor β signaling pathway represses skeletal muscle growth and promotes muscle wasting, a role in muscle for the parallel bone morphogenetic protein (BMP) signaling pathway has not been defined. We report, for the first time, that the BMP pathway is a positive regulator of muscle mass. Increasing the expression of BMP7 or the activity of BMP receptors in muscles induced hypertrophy that was dependent on Smad1/5-mediated activation of mTOR signaling. In agreement, we observed that BMP signaling is augmented in models of muscle growth. Importantly, stimulation of BMP signaling is essential for conservation of muscle mass after disruption of the neuromuscular junction. Inhibiting the phosphorylation of Smad1/5 exacerbated denervation-induced muscle atrophy via an HDAC4-myogenin–dependent process, whereas increased BMP–Smad1/5 activity protected muscles from denervation-induced wasting. Our studies highlight a novel role for the BMP signaling pathway in promoting muscle growth and inhibiting muscle wasting, which may have significant implications for the development of therapeutics for neuromuscular disorders.

Introduction

In developing and adult mammalian skeletal muscle, the TGF-β signaling network functions as a dominant repressor of protein anabolism and a principal driver of protein catabolism underlying muscle wasting. These effects have been attributed to TGF-β family members (most notably myostatin and activin) that engage activin receptors and stimulate the Smad2/3 signaling proteins to mediate the transcriptional activity of genes controlling cell size. Inhibition of the myostatin/activin–Smad2/3 axis has been proposed as a potential therapeutic strategy for treating conditions associated with loss of muscle mass and strength as (a) deletion of myostatin (Kambadur et al., 1997; McPherron et al., 1997; Lee and McPherron, 2001; Lee, 2007); (b) antagonism of myostatin by inhibitory proteins, antibodies, or soluble activin receptors (Bogdanovich et al., 2002; Zhou et al., 2010; Winbanks et al., 2012); or (c) inhibition of Smad2/3 (Sartori et al., 2009; Winbanks et al., 2012) can promote muscle growth and ameliorate muscle wasting. Within the TGF-β network, the parallel signaling axis controlled by bone morphogenetic proteins (BMPs) regulates the transcription of target genes distinct to those regulated by the myostatin/activin–Smad2/3 axis (Massagué et al., 2005). Although some studies suggest that BMP signaling may regulate embryonic muscle development (Pourquié et al., 1996; Amthor et al., 1998) or the regeneration of skeletal muscle (Clever et al., 2010; Ruschke et al., 2012), research to date provides limited insight into whether or not BMP signaling operates in postmitotic myofibers to directly regulate the skeletal muscle phenotype.

BMP ligands engage specific membrane-bound serine/threonine kinase receptors that convey signals to intracellular Smad proteins 1, 5, and 8. Phosphorylation of Smad1/5/8

Correspondence to Paul Gregorevic: paul.gregorevic@bakeridi.edu.au; or Catherine Winbanks: catherine.winbanks@bakeridi.edu.au

Abbreviations used in this paper: BMP, bone morphogenetic protein; H&E, hematoxylin and eosin; IGF, insulin-like growth factor; TA, tibialis anterior.

The Rockefeller University Press $30.00
J. Cell Biol. Vol. 203 No. 2 345–357
www.jcb.org/cgi/doi/10.1083/jcb.201211134

by BMP-stimulated receptors promotes complex formation with Smad4 and nuclear retention where, in cooperation with transcriptional coregulators, they govern gene expression in a cell- and context-dependent manner (Massagué et al., 2005). BMP signaling is negatively regulated by Smad proteins 6 and 7, which prevent receptor-mediated activation of Smad1/5/8 (Hayashi et al., 1997; Imamura et al., 1997; Nakao et al., 1997). The complexity of the TGF-β signaling network includes cross-regulation between the myostatin/activin–Smad2/3 and BMP–Smad1/5/8 axes. Ligands can compete for common serine/threonine kinase receptors (Donaldson et al., 1992; Mathews et al., 1992; Rebbapragada et al., 2003; Sako et al., 2010) to promote formation of so-called mixed R-Smad complexes (e.g., Smad1/3/5) that can activate and perturb the transcription of respective TGF-β and BMP target genes (Grönroos et al., 2012). Thus, the canonical TGF-β and BMP signaling axes have the potential to operate in parallel and reciprocally.

Based on the pivotal role that the myostatin/activin–Smad2/3 axis plays in regulating skeletal muscle mass and the hypothesized parallel operation of TGF-β and BMP signaling, we sought to determine the role of the BMP–Smad1/5/8 signaling pathway in the regulation of skeletal muscle growth and wasting. In contrast to the established negative influence of the myostatin/activin–Smad2/3 axis on muscle mass, herein we identify the BMP–Smad1/5/8 axis as a positive regulator of skeletal muscle mass in vivo, promoting muscle growth and preventing muscle wasting. Interventions that stimulate the BMP–Smad1/5/8 signaling axis may offer therapeutic benefits in preventing or ameliorating pathology associated with muscle wasting.

Results

BMP ligands and BMP receptor activation promotes skeletal muscle hypertrophy

To determine whether the BMP axis can regulate postnatal skeletal muscle growth, we designed rAAV6 vectors encoding BMP7 (rAAV6:BMP7) or a constitutively active type I BMP receptor (rAAV6:ALK3). rAAV6:BMP7 and rAAV6:ALK3 significantly increased the activity of a BMP luciferase reporter construct transfected into C2C12 cells (Fig. 1 a). When delivered to mouse tibialis anterior (TA) hindlimb muscles, rAAV6:BMP7 and rAAV6:ALK3 increased BMP7 and ALK3 protein and mRNA expression, respectively (Fig. 1 b), and increased Smad1/5$^{S463/465}$ phosphorylation (Fig. 1 c). Significantly, administration of rAAV6:BMP7 and rAAV6:ALK3 to the TA muscles of 8-wk-old mice considerably increased skeletal muscle mass within 28 d of injection (Fig. 1 d). Histological examination revealed that the increase in muscle mass after rAAV6:BMP7 or rAAV6:ALK3 administration was a product of muscle fiber hypertrophy (Fig. 1 e), as demonstrated by increases in myofiber diameter and area (Fig. 1 f). We also determined that muscles injected with rAAV6:BMP7 or rAAV6:ALK3 demonstrated increased transcription of insulin-like growth factor (IGF) isoforms, which can promote striated muscle growth (Musarò et al., 1999; Kalista et al., 2012; Fig. 1 g and Fig. S1 a). As IGF proteins can potentiate PI3K/Akt/mTOR signaling (Rommel et al., 2001), we also determined that rAAV6:BMP7 and rAAV6:ALK3 increased the phosphorylation of pAkt^{S473}, mTOR^{S2448}, and the downstream targets S6RP$^{S235/236}$ and 4EBP1$^{T37/46}$ (Fig. 1 h). We did not observe altered abundance or phosphorylation of Foxo1/3, or expression of the muscle-specific E3 ligases MuRF1 and Atrogin1 in response to rAAV6:BMP7 (Fig. S1, b and c), demonstrating that hypertrophy driven by enhancing BMP signaling in healthy muscles is not a product of altering this key mechanism of muscle protein degradation. As the activity of mTOR is a key regulator of protein synthesis in muscle, we sought to determine whether muscle growth induced by BMP signaling was dependent on activation of mTOR. We established that rAAV6:BMP7-induced S6RP$^{S235/236}$ phosphorylation was completely ablated by coadministration of rapamycin (Fig. 1 i), a specific inhibitor of mTORC1 signaling (Heitman et al., 1991; Chung et al., 1992). Rapamycin completely prevented rAAV6:BMP7-induced increases in muscle mass and myofiber size (Fig. 1, j and k; and Fig. S1 d), despite continued overexpression of BMP7 (Fig. S1, e and f) and increased phosphorylation of Smad1/5 (Fig. S1 g). These data constitute the first demonstration that the BMP signaling axis is a bona fide regulator of skeletal muscle growth and that the mTORC1 pathway is indispensable in this process.

BMP7-induced skeletal muscle hypertrophy is mediated by Smad1/5/8

To directly test the role of the BMP-regulated Smads (Smad1/5/8) in the regulation of muscle hypertrophy, we designed an rAAV6 vector encoding Smad6 (rAAV6:Smad6), which inhibits phosphorylation of BMP-regulated Smads (Imamura et al., 1997; Ishida et al., 2000). In cultures of C2C12 cells, Smad6 potently blocked BMP4-induced activation of a BMP activity-sensing luciferase reporter (Fig. 2 a). Administration of rAAV6:Smad6 in vivo potently suppressed the phosphorylation of Smad1/5$^{S463/465}$ in TA muscles, but did not alter the mass of muscles examined 28 d after administration (Fig. 2 b and Fig. S2, a and b). To test the importance of the BMP-regulated Smads in controlling BMP7-induced hypertrophy, rAAV6:Smad6 was codelivered with rAAV6:BMP7 to the TA muscles of mice. At 28 d after administration, Smad6 had completely prevented muscle hypertrophy (Fig. 2, b and c) and increases in myofiber size (Fig. 2 d) normally induced by rAAV6:BMP7. As predicted, Smad6 potently suppressed BMP7-induced phosphorylation of Smad1/5$^{S463/465}$ (Fig. 2 e). Importantly, we found that rAAV6:Smad6 also suppressed BMP7-induced phosphorylation of Akt^{S473}, mTOR^{S2448}, S6RP$^{S235/236}$, and 4EBP1$^{T37/46}$ (Fig. 2 f). Administration of rAAV6:Smad6 alone did not affect mTOR signaling (Fig. S2 c). These data demonstrate that the BMP signaling axis regulates skeletal muscle mass via the activation of Smads1/5/8 and that the suppression of BMP-regulated Smads by Smad6 can inhibit mTOR activation downstream of Smad1/5, which is required for muscle hypertrophy.

Endogenous BMP signaling is altered in models of muscle growth

To further explore the significance of the BMP axis as a regulator of skeletal muscle growth, we analyzed Smad1/5$^{S463/465}$ phosphorylation in skeletal muscles undergoing hypertrophy.

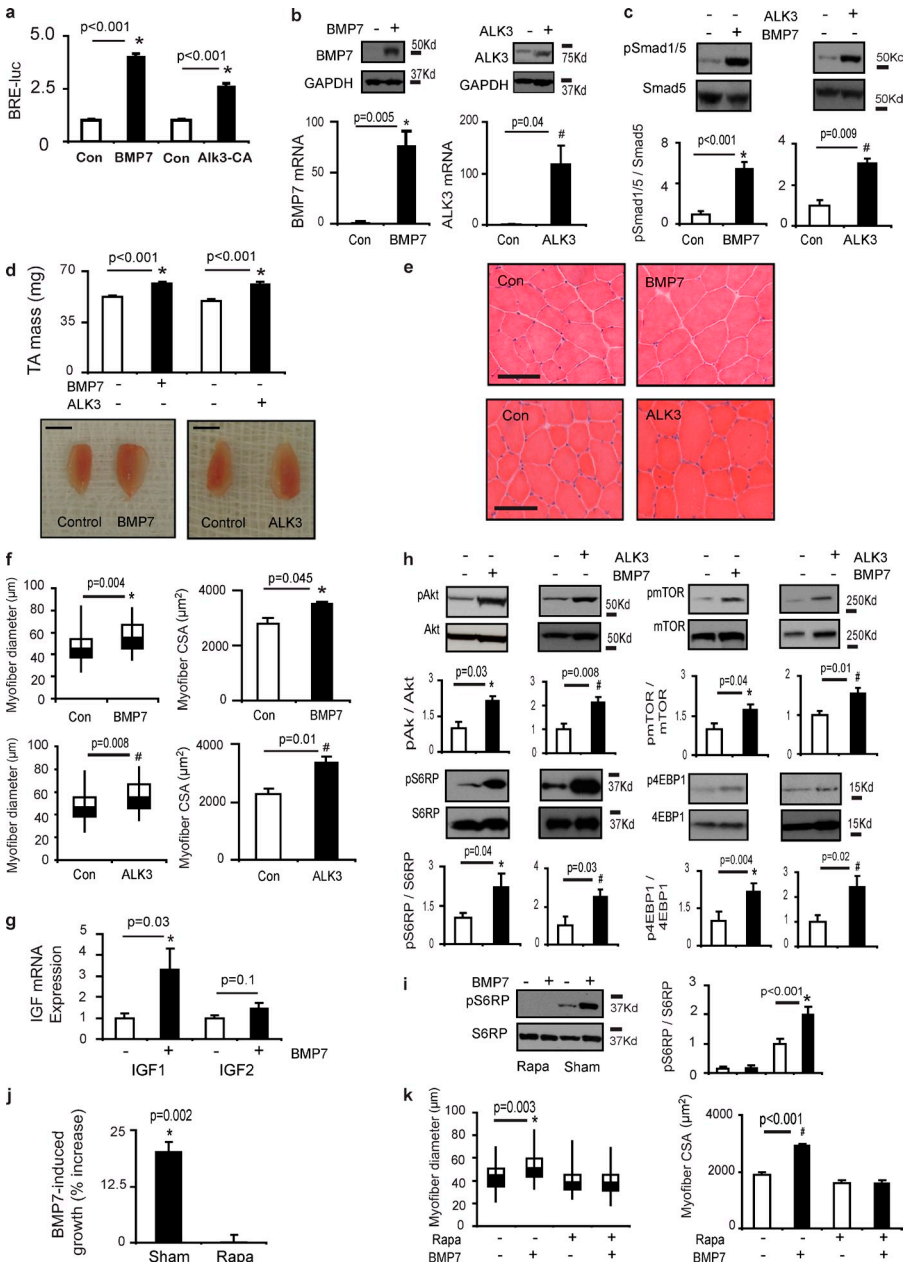

Figure 1. **Postnatal expression of BMP7 and ALK3 promotes skeletal muscle hypertrophy.** (a) Plasmids expressing BMP7 or constitutively active type-IA BMP receptor (ALK3) were transfected into C2C12 cells along with plasmids expressing a BMP luciferase reporter and β-galactosidase 48 h before examination (*, P < 0.001 vs. control). Figure represents three independent experiments, with each individual experiment performed in triplicate. (b) The administration of rAAV6:BMP7 or rAAV6:ALK3 to mouse limb muscles resulted in significant increases in BMP7 (n = 4 per treatment) and ALK3 (n = 4 per treatment) protein and gene expression, respectively, when examined 28 d after injection (*, P = 0.005 vs. control; #, P = 0.04 vs. control). (c) rAAV6:BMP7 (n = 4 per treatment) and rAAV6:ALK3 (n = 4 per treatment) significantly increased the phosphorylation of Smad1/5$^{S463/465}$ (*, P < 0.001 vs. control; #, P = 0.009 vs. control). (d) Injection of the anterior musculature of the mouse hindlimb with rAAV6:BMP7 (n = 11) or rAAV6:ALK3 (n = 4 per treatment) increased muscle mass by ~25% (*, P < 0.001 vs. control). Bars, 5 mm. (e and f) Muscle hypertrophy was a product of increased muscle fiber size as demonstrated by representative H&E-stained cryosections and quantification of myofiber diameter (represented as box and whisker plots comprising minimum, lower quartile, median, upper quartile, and maximum values for myofiber diameter; *, P = 0.004 vs. control; #, P = 0.008 vs. control) and myofiber area (*, P = 0.045 vs. control; #, P = 0.01 vs. control; n = 3 per treatment). Bars, 100 µm. (g) IGF1 and IGF2 mRNA expression was determined 28 d after rAAV6:BMP7 administration (*, P = 0.03 vs. control; n = 7–9 per treatment). (h) Muscles examined 28 d after injection of rAAV6:BMP7 (n = 5–8 per treatment) or rAAV6:ALK3 (n = 4–11 per treatment) demonstrated significant increases in phosphorylation of Akt^{S473} (*, P = 0.03 vs. control; #, P = 0.008 vs. control), mTOR^{S2448} (*, P = 0.04 vs. control; #, P = 0.01 vs. control), S6RP$^{S235/236}$ (*, P = 0.04 vs. control; #, P = 0.03 vs. control), and 4EBP1$^{T37/46}$ (*, P = 0.004 vs. control; #, P = 0.02 vs. control). (i) When administered at 1 mg/kg/day, rapamycin attenuated BMP7-induced phosphorylation of S6RP$^{S235/236}$ when compared with muscles expressing BMP7 that were collected with animals receiving vehicle (*, P < 0.001 vs. control; n = 4–5 per treatment). (j) Intraperitoneal injections of rapamycin for 28 d completely prevented the ability of BMP7 (n = 5–7 per treatment) to induce skeletal muscle growth. The muscle hypertrophy induced by BMP7 is presented as a percentage increase in the presence of either sham or rapamycin (*, P = 0.002 vs. control). (k) Increases in myofiber diameter and area typically observed in muscles examined 28 d after injection of rAAV6:BMP7 were prevented by coadministration of rapamycin (*, P = 0.003 vs. control; #, P < 0.001 vs. control; n = 3 per treatment). Data for myofiber diameter are presented as box and whisker plots comprising minimum, lower quartile, median, upper quartile, and maximum values. Data are presented as means ± SEM.

We found that in skeletal muscles expressing follistatin (via rAAV6:Fst-288 injection), a protein that promotes hypertrophy by preventing myostatin and activin from engaging activin receptors (Lee, 2007; Lee et al., 2010; Winbanks et al., 2012), Smad1/5$^{S463/465}$ phosphorylation was increased (Fig. S3 a). The increases in Smad1/5$^{S463/465}$ phosphorylation were associated with decreased Smad6 expression in muscles undergoing follistatin-induced hypertrophy (Fig. S3 b). When we coadministered rAAV6:Smad6 with rAAV6:Fst-288 to the TA muscles of mice, follistatin-induced hypertrophy of muscle fibers was profoundly blunted (Fig. S3, c–e). We confirmed that increased expression of Smad6 significantly suppressed the phosphorylation of Smad1/5 in response to follistatin overexpression (Fig. S3 f). Previously, we established that follistatin-mediated muscle hypertrophy promotes activation of the Akt/mTOR/S6RP/4EBP cascade to stimulate protein synthesis (Winbanks et al., 2012). Here, the suppression of follistatin-mediated muscle hypertrophy by rAAV6:Smad6 suppressed the phosphorylation of Akt^{S473}, mTOR^{S2448}, S6RP$^{S235/236}$, and 4EBP1$^{T37/46}$ (Fig. S3 g). These results demonstrate that hypertrophy of skeletal muscle can involve recruitment of the BMP signaling pathway.

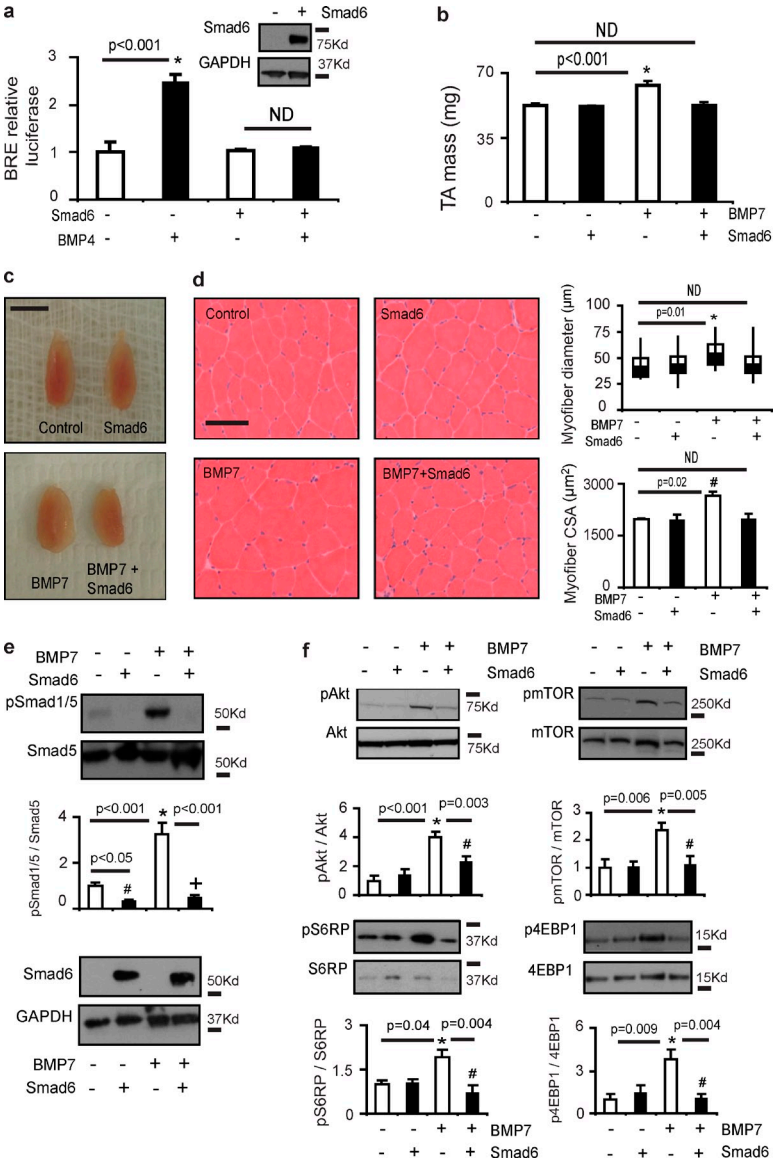

Figure 2. **BMP7-induced skeletal muscle growth is mediated by Smad1/5.** (a) rAAV6:Smad6 was applied to C2C12 cells to determine its ability to suppress BMP4-induced BRE-luciferase activity. After administration of vector, cells were treated for 24 h with 3 nM BMP4 and then lysed to assess luciferase activity (*, $P < 0.001$ vs. control). Figure represents three independent experiments, with each individual experiment performed in triplicate. (b) The coadministration of rAAV6:Smad6 with rAAV6:BMP7 significantly attenuated BMP7-induced hypertrophy in mouse limb muscles, as determined by changes in TA muscle mass (*, $P < 0.001$ vs. control). Muscles expressing both BMP7 and Smad6 did not differ compared with control muscles when examined 28 d after injection (ND, not different). $n = 4–10$ per treatment. (c) Image of TA muscles demonstrating BMP7-induced hypertrophy and the inhibitory effect of Smad6 coexpression. Bar, 5 mm. (d) Representative images and myofiber diameter and area quantification demonstrate that BMP7-induced myofiber hypertrophy is significantly suppressed by Smad6 (*, $P = 0.01$ vs. control; #, $P = 0.02$ vs. control; $n = 3$ per treatment). Myofiber diameter is presented as box and whisker plots comprising minimum, lower quartile, median, upper quartile, and maximum values for myofiber diameter. Muscles coexpressing BMP7 and Smad6 were not different from control muscles 28 d after injection (ND, not different). Bar, 100 µm. (e) Smad6 coadministration reduced the phosphorylation of Smad1/5$^{S463/465}$ normally induced 28 d after injection of rAAV6:BMP7 alone, as determined by Western blot analysis (*, $P < 0.001$ vs. control; #, $P < 0.05$ vs. control; +, $P < 0.001$ vs. BMP7-treated muscles; $n = 5–10$ per treatment). (f) Smad6 coadministration reduced the phosphorylation of Akt^{S473} (*, $P < 0.001$ vs. control; #, $P = 0.003$ vs. BMP7 treatment), mTOR^{S2448} (*, $P = 0.006$ vs. control; #, $P = 0.005$ vs. BMP7 treatment), S6RP$^{S235/236}$ (*, $P = 0.04$ vs. control; #, $P = 0.004$ vs. BMP7 treatment), and 4EBP1$^{T37/46}$ (*, $P = 0.009$ vs. control; #, $P = 0.004$ vs. BMP7 treatment) when compared with the effect of BMP7 alone. $n = 4–8$ per treatment. Data are presented as means ± SEM.

Differential BMP–Smad1/5 signaling in muscle development and disease

As BMP signaling promotes hypertrophy of mature skeletal muscle fibers, we considered whether the activity of this pathway contributes to muscle growth during postnatal maturation and becomes affected in muscle wasting conditions. Skeletal muscle protein synthesis in rodents is highest up to 1 wk after birth, before progressively declining to stable adult levels (Suryawan et al., 2006). We found that the phosphorylation of Smad1/5$^{S463/465}$ declined markedly from 1 wk after birth until 6 mo of age (Fig. 3 a), consistent with BMP signaling participating in the development of skeletal musculature. To determine the role of BMP signaling in skeletal muscle wasting, we examined Smad1/5 phosphorylation in muscles exhibiting wasting associated with motor nerve degeneration, transection, or blockade. In TA muscles from rats subjected to intensive care disuse for up to 9 d, Smad1/5$^{S463/465}$ phosphorylation was increased coincident with a decrease in TA mass (Fig. 3 b). Similarly, Smad1/5$^{S463/465}$ phosphorylation was markedly increased in TA muscles from mice modeling amyotrophic lateral sclerosis (via a mutation in the superoxide dismutase gene, designated SOD1^{G93A}) at ages preceding marked loss of muscle mass (60 d) or coinciding with observable muscle atrophy (90 d; Gurney et al., 1994; Fig. 3 c). Confirming that Smad1/5 phosphorylation increases in muscles when motor nerve activity is compromised, we also detected striking increases in Smad1/5$^{S463/465}$ phosphorylation in TA muscles from mice subjected to motor nerve resection (Fig. 3 d). Smad1/5 phosphorylation was increased in muscles as early as 3 d after denervation and remained increased for at least 14 d after denervation (Fig. 3 d). To explore why Smad1/5$^{S463/465}$ phosphorylation was increased in response to loss of nerve supply to skeletal muscle, we profiled the expression of the BMP pathway components in denervated skeletal muscles. We identified profoundly increased transcription of the BMP receptor ligands GDF5 (BMP14) and GDF6 (BMP13) and the type-IB BMP receptor (ALK6; Fig. 3, e and f), but not other BMP ligands (Fig. S4 a) or the type-IA BMP receptor (ALK3; Fig. 3 f). We also found that transcription of Smad6 and Noggin, the latter

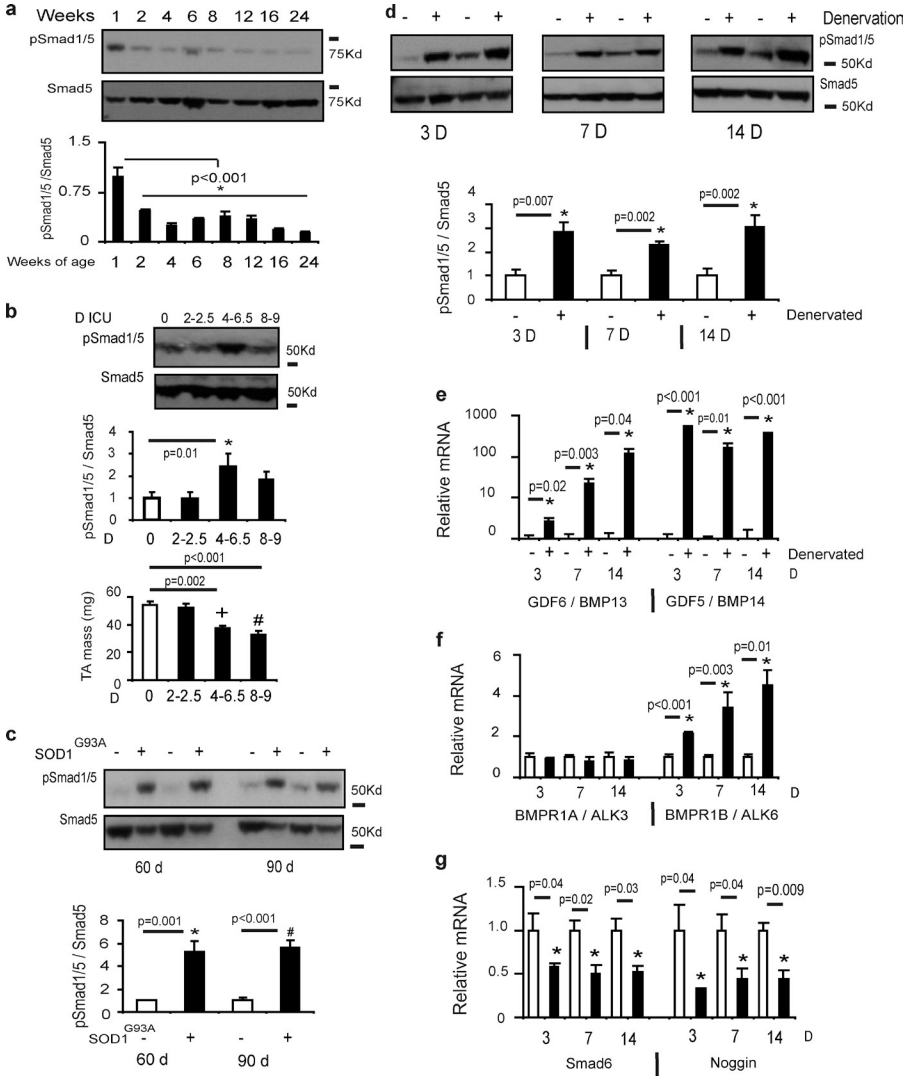

Figure 3. **Endogenous BMP signaling is altered in models of skeletal muscle growth and wasting.** (a) TA muscles were collected from neonatal and young adult mice and the phosphorylation of Smad1/5 was determined by Western blotting (*, P < 0.001 vs. control). *n* = 3 per time point. (b) Rats subjected to intensive care immobilization (*n* = 3–6 per treatment) displayed muscle atrophy with increased phosphorylation of pSmad1/5 (*, P = 0.01 vs. control muscles; +, P = 0.002 vs. control muscles; #, P < 0.001 vs. control muscles). (c) Smad1/5$^{S463/465}$ phosphorylation was assessed in mice (*n* = 5 per treatment) with a SOD1^{G93A} mutation that displays symptoms akin to amyotrophic lateral sclerosis patients. At a time point before the onset of muscle atrophy (60 d; *, P = 0.001 vs. control) and at a point of advanced pathology (90 d; #, P < 0.001 vs. control) Smad1/5 phosphorylation was increased. (d) Smad1/5$^{S463/465}$ phosphorylation was assessed by Western blot 3 d (*n* = 5 per treatment; *, P = 0.007 vs. control), 7 d (*n* = 6 per treatment; *, P = 0.002 vs. control), and 14 d (*n* = 5–6 per treatment; *, P = 0.002 vs. control) after excision of a portion of the peroneal nerve supplying the TA muscle in wild-type mice. (e–g) mRNA expression of GDF6 (BMP13), GDF5 (BMP14), BMPR1A, BMPR1B, Smad6, and Noggin was assessed by RT-PCR (*n* = 4–6 per treatment; see specific time points for p-values). Gene expression was analyzed using the ΔΔCT method of analysis and expression was normalized to 18S. Data are presented as means ± SEM.

of which antagonizes extracellular BMP ligands (Holley et al., 1996; Zimmerman et al., 1996), was suppressed at all time points examined after denervation where Smad1/5$^{S463/465}$ phosphorylation was increased (Fig. 3 g). The transcription of other BMP axis repressors including Smad7, Smurf1/2, or Chordin was not altered (Fig. S4 b). These data identify that the expression of BMP axis elements is altered to promote Smad1/5$^{S463/465}$ phosphorylation in muscles exhibiting wasting associated with motor nerve transaction, degeneration, or disuse.

BMP signaling protects skeletal muscle from denervation-induced atrophy

Having identified that phosphorylation of Smad1/5 is increased in muscles undergoing wasting associated with nerve transection, degeneration, and inactivity, we next sought to determine the functional role of increased Smad1/5$^{S463/465}$ phosphorylation in the muscles' response to denervation. Because Smad6 is an endogenous inhibitor of Smad1/5 phosphorylation and we found that its expression decreased in denervation, we administered rAAV6:Smad6 to muscles at the time of motor nerve resection to prevent BMP–Smad1/5 signaling. Strikingly, we found that the administration of rAAV6:Smad6 considerably exacerbated atrophy of denervated muscles, compared with denervation alone (Fig. 4, a–c). Importantly, increased Smad6 expression potently suppressed Smad1/5 phosphorylation in denervated muscles (Fig. 4 d), confirming that inhibition of Smad1/5 phosphorylation is associated with the exacerbation of denervation-induced muscle atrophy. Supporting this concept, we showed that pretreatment of TA muscles with rAAV6:BMP7 28 d before denervation reduced muscle loss (Fig. 4 e) and decreases in myofiber size (Fig. 4, f and g). Administration of rAAV6:ALK3 also reduced denervation-induced muscle atrophy and preserved myofiber size (Fig. 4, h–j). These data demonstrate that augmented BMP–Smad1/5 signaling performs a critical role in limiting muscle wasting associated with denervation.

The BMP signaling axis regulates the expression of E3 ligases via the HDAC4–myogenin axis associated with neurogenic atrophy

To gain insight into how the BMP signaling pathway may prevent neurogenic muscle wasting, we examined denervated skeletal muscles treated with rAAV6:Smad6 for changes in the expression of E3 ubiquitin ligases. The ubiquitination of protein

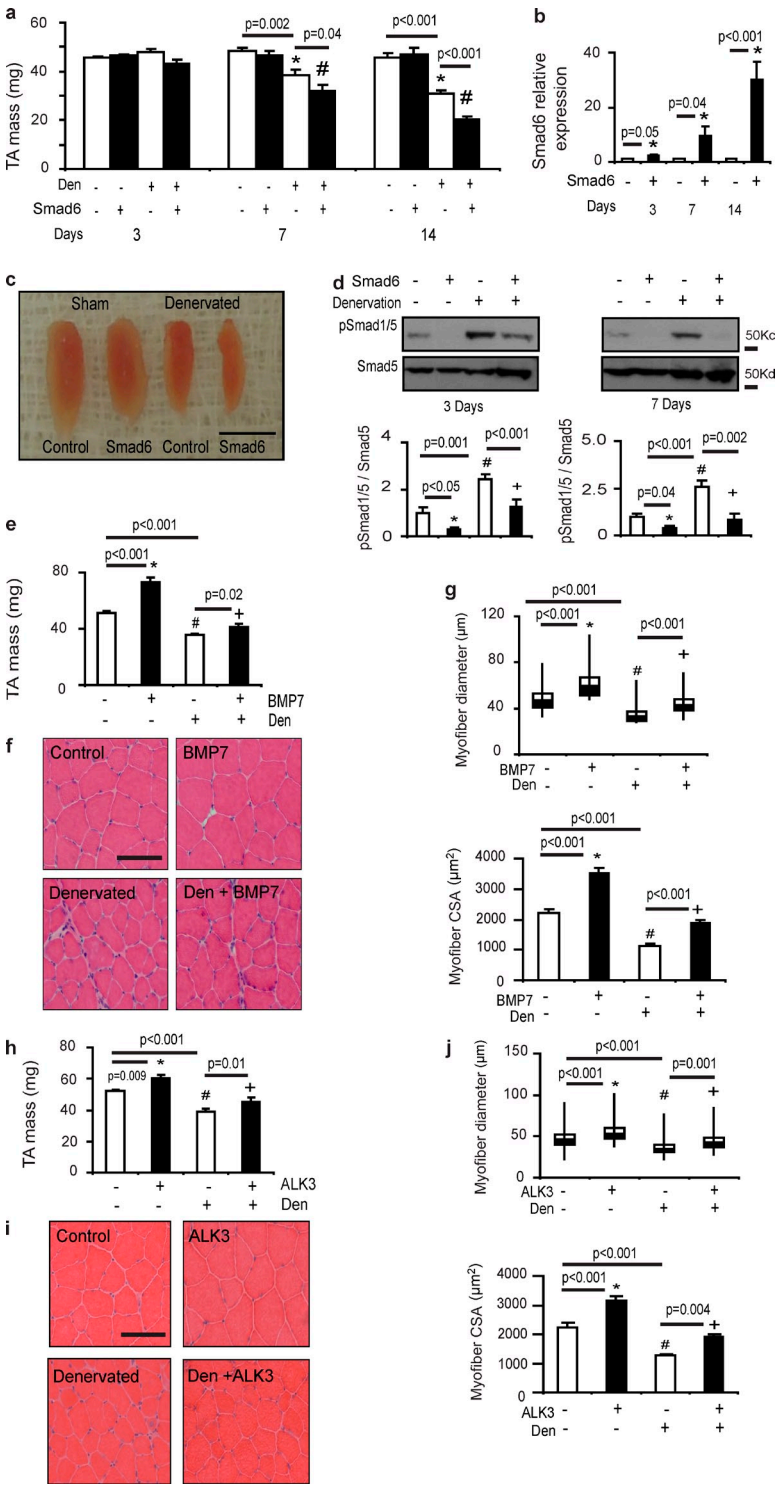

Figure 4. **BMP signaling protects skeletal muscle from wasting in denervation.** (a) rAAV6:Smad6 was delivered to the TA muscles immediately after denervation. Muscle masses were then assessed 3 d (n = 6 per treatment), 7 d (n = 5–6 per treatment; *, P = 0.002 vs. control; #, P = 0.04 vs. denervation), and 14 d (n = 4–6 per treatment; *, P < 0.001 vs. control; #, P < 0.001 vs. denervation) after denervation. (b) Smad6 gene expression increased at 3 d (n = 6 per treatment; *, P = 0.05 vs. control), 7 d (n = 5 per treatment; *, P = 0.04 vs. control), and 14 d (n = 6 per treatment; *, P < 0.001 vs. control) after injection in denervated TA muscles. (c) Denervated TA muscles treated with rAAV6:Smad6 appeared smaller than denervated muscles 14 d after denervation. Bar, 5 mm. (d) Expression of Smad6 in TA muscles denervated for 3 d (n = 5–10 per treatment; *, P < 0.05 vs. control; #, P = 0.001 vs. control; +, P < 0.001 vs. denervation) and 7 d (n = 6–12 per treatment; *, P = 0.04 vs. control; #, P < 0.001 vs. control; +, P = 0.002 vs. denervation) correlated with suppression of Smad1/5$^{S463/465}$ phosphorylation, as determined by Western blotting. (e) TA muscles were pretreated with rAAV6:BMP7 for 28 d and then denervated 14 d before tissue collection. Although denervation induced ∼30% loss of muscle mass, increased expression of BMP7 significantly diminished muscle atrophy (n = 3 sham and 6 den; *, P < 0.001 vs. control; #, P < 0.001 vs. control; +, P = 0.02 vs. denervation). (f and g) Representative H&E images and quantification of myofiber diameter and area demonstrates that loss of myofiber diameter (*, P < 0.001 vs. control; #, P < 0.001 vs. control; +, P < 0.001 vs. denervation) and area (*, P < 0.001 vs. control; #, P < 0.001 vs. control; +, P < 0.001 vs. den, n = 3 per treatment) after denervation can be ameliorated by rAAV6:BMP7 administration. Myofiber diameter is presented as box and whisker plots comprising minimum, lower quartile, median, upper quartile, and maximum values for myofiber diameter. (h) TA muscles were pretreated with rAAV6:ALK3 for 28 d and then denervated 14 d before sample collection. rAAV6:ALK3 significantly reduced muscle atrophy (n = 3 sham and 4 den; *, P = 0.009 vs. control; #, P < 0.001 vs. control; +, P = 0.01 vs. denervation). (i and j) Representative H&E images and quantification of myofiber diameter and area demonstrates that loss of myofiber diameter (*, P < 0.001 vs. control; #, P < 0.001 vs. control; +, P = 0.001 vs. denervation) and area (*, P < 0.001 vs. control; #, P < 0.001 vs. control; +, P = 0.004 vs. den; n = 3 per treatment) after denervation can be diminished by rAAV6:ALK3 administration. Myofiber diameter is presented as box and whisker plots comprising minimum, lower quartile, median, upper quartile, and maximum values for myofiber diameter. Bar, 100 μm. Data are presented as means ± SEM.

targets (such as contractile proteins) by specific E3 ligases including MuRF1 and atrogin1 plays a key role in proteasome-mediated protein degradation associated with muscle wasting (Bodine et al., 2001; Cohen et al., 2009). We found that the transcription of MuRF1 and atrogin1 was increased in denervated muscles transduced with rAAV6:Smad6, compared with denervated muscles receiving a sham vector (Fig. 5 a). Profiling of gene expression associated with sarcopenic wasting in old rats (where progressive motor nerve loss occurs) recently documented up-regulation of another E3 ubiquitin ligase, Fbxo30, in correlation with markers of motor nerve degeneration (Ibebunjo et al., 2013). Emerging evidence points to Fbxo30 (also referred to as Musa1) as a novel atrophy-associated E3 ligase in skeletal muscle (Sartori et al., 2013). We found transcription of Fbxo30/Musa1 was increased in denervated muscles at all time points examined after nerve resection (Fig. 5 a). Even more significantly, the expression of Fbxo30/Musa1 was markedly potentiated in denervated muscles in association with exacerbated atrophy when

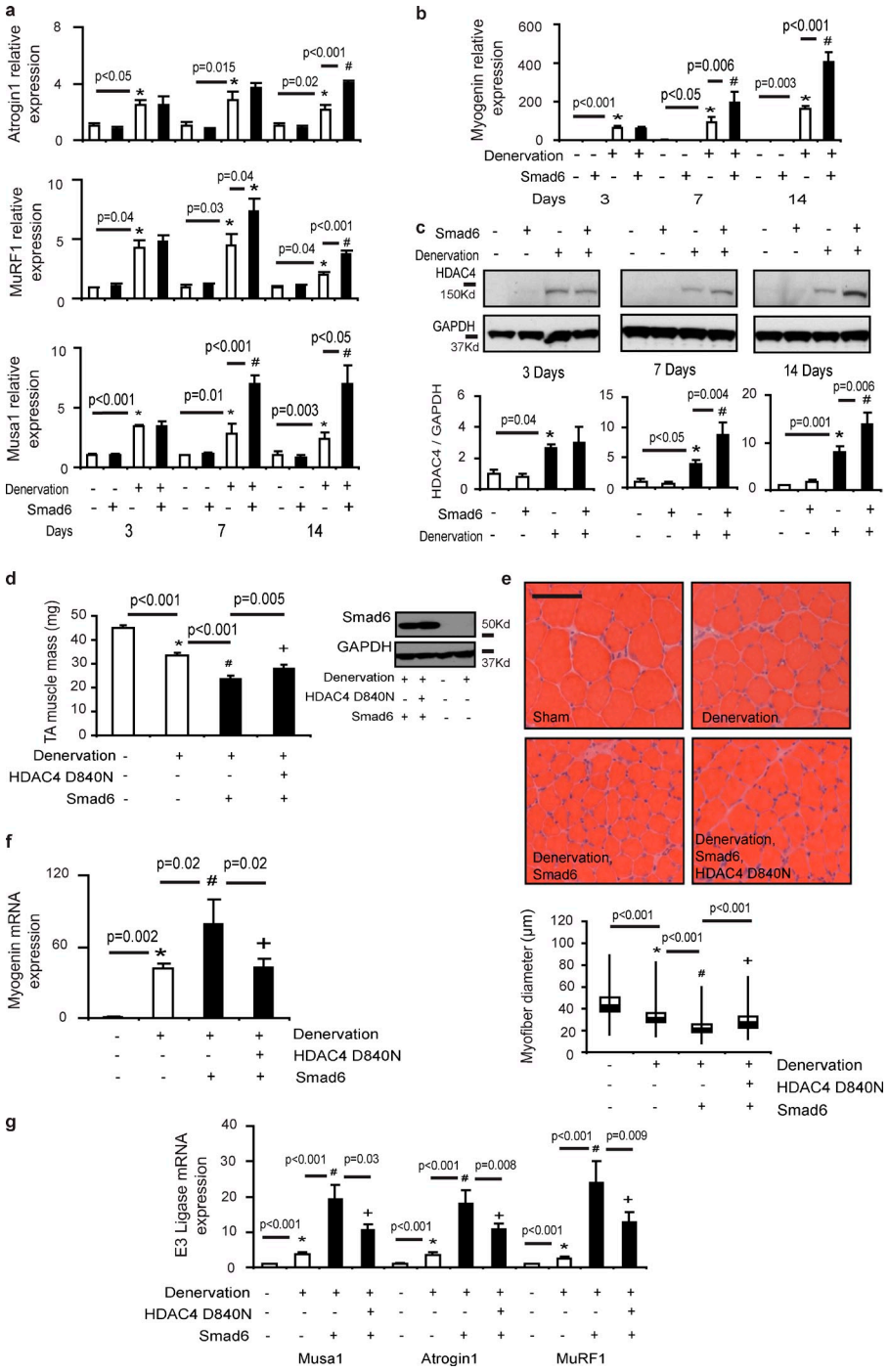

Figure 5. **The BMP signaling axis regulates the expression of E3 ubiquitin ligases via the HDAC4–myogenin axis in neurogenic muscle wasting.** (a) The E3 ligase atrogin1 was detected by RT-PCR 3 d (n = 3–6 per treatment; *, P < 0.05 vs. control), 7 d (n = 3–5 per treatment; *, P = 0.015 vs. control), and 14 d (n = 3–6 per treatment; *, P = 0.02 vs. control; #, P < 0.001 vs. denervation) after denervation. MuRF1 gene expression was detected by RT-PCR at 3 d (n = 3–6 per treatment; *, P = 0.04 vs. control), 7 d (n = 3–5 per treatment; *, P = 0.03 vs. control; #, P = 0.04 vs. denervation), and 14 d (n = 3–6 per treatment; *, P = 0.04 vs. control; #, P < 0.001 vs. denervation) after denervation. Fbxo30/MUSA1 expression was detected at 3 d (n = 6 per treatment; *, P < 0.001 vs. control), 7 d (n = 5–6 per treatment; *, P = 0.01 vs. control; #, P < 0.001 vs. denervation), and 14 d (n = 4–6 per treatment; *, P = 0.003 vs. control; #, P < 0.05 vs. denervation) after denervation via RT-PCR. (b) Myogenin was measured at 3 d (n = 6 per treatment; *, P < 0.001 vs. control), 7 d (n = 5–6 per treatment; *, P < 0.05 vs. control; #, P = 0.006 vs. denervation), and 14 d (n = 3–6 per treatment; *, P = 0.003 vs. control; #, P < 0.001 vs. denervation) after denervation via RT-PCR. (c) HDAC4 protein expression was analyzed by Western blotting at 3 d (n = 3–4 per treatment; *, P = 0.04 vs. control), 7 d (n = 6–9 per treatment; *, P < 0.05 vs. control; #, P = 0.004 vs. denervation), and 14 d (n = 4–8 per treatment; *, P = 0.001 vs. control; #, P = 0.006 vs. denervation) after denervation and normalized to GAPDH levels. (d) A dominant-negative HDAC4 mutant ($HDAC^{D840N}$) was coadministered with rAAV6:Smad6 in denervated muscles for 8 d. Western blotting demonstrates that Smad6 protein expression was not affected by coadministration of rAAV6:Smad6 with $rAAV6:HDAC4^{D840N}$ (n = 5–9 per treatment; *, P < 0.001 vs. control; #, P < 0.001 vs. den; +, P = 0.005 vs. Smad6 in denervation). (e) Representative H&E stained images demonstrate that myofiber size is increased when rAAV6:Smad6 is coadministered with $rAAV6:HDAC4^{D840N}$, as verified by quantification of myofiber diameter. Bar, 100 µm. Myofiber diameter is presented as box and whisker plots comprising minimum, lower quartile, median, upper quartile, and maximum values (n = 3 per treatment; *, P < 0.001 vs. control; #, P < 0.001 vs. den; +, P < 0.001 vs. Smad6 in denervation). (f) Myogenin (*, P = 0.002 vs. control; #, P = 0.02 vs. den; +, P = 0.02 vs. Smad6 in denervation) gene expression was determined using TaqMan gene expression assays 8 d after denervation (n = 5–10 per treatment). (g) E3 ligases including Fbxo30/MUSA1 (*, P < 0.001 vs. control; #, P < 0.001 vs. den; +, P = 0.03 vs. Smad6 in denervation), atrogin1 (*, P < 0.001 vs. control; #, P < 0.001 vs. den; +, P = 0.008 vs. Smad6 in denervation), and MuRF1 (*, P < 0.001 vs. control; #, P < 0.001 vs. den; +, P = 0.009 vs. Smad6 in denervation) were also measured in muscles collected 8 d after denervation (n = 5–10 per treatment). Data are presented as means ± SEM.

BMP–Smad1/5 signaling was inhibited by administration of rAAV6:Smad6 (Fig. 5 a).

We sought to determine how changes in BMP–Smad1/5 signaling regulate transcription of the aforementioned E3 ligases that contribute to proteolysis in muscles. Expression of MuRF1 and atrogin1 is promoted by nuclear translocation of the FoxO proteins (Sandri et al., 2004), which, in turn, is repressed by Akt kinase activity (Sandri et al., 2004; Stitt et al., 2004; Latres et al., 2005). However, we found that rAAV6:Smad6 did not alter phosphorylation of $FoxO1^{T24}$/$FoxO3a^{T32}$ or affect Akt^{S473} phosphorylation in denervated muscles (Fig. S4 c). As an alternate mechanism, we assessed the HDAC4–myogenin axis, as deletion of either HDAC4 or myogenin renders skeletal muscles resistant to neurogenic atrophy and prevents the up-regulation of MuRF1 and atrogin1 (Tang et al., 2009; Moresi et al., 2010). Strikingly, we found that inhibiting BMP–Smad1/5 signaling in

denervated muscles via the administration of rAAV6:Smad6 robustly increased the transcription of myogenin when compared with the effect of denervation alone (Fig. 5 b). Further supporting a role for the HDAC4–myogenin axis as a target for repression by phosphorylated Smad1/5 in denervated muscles, we observed that HDAC4 gene and protein expression were significantly increased when BMP signaling was inhibited by rAAV6:Smad6 administration after nerve resection (Fig. 5 c and Fig. S5 a). We generated an rAAV6 vector designed to express a HDAC4 mutant (HDAC4^{D840N}) in which a single base pair mutation abrogates physical interaction with HDAC3, thereby abolishing the activity of HDAC4 (Fischle et al., 2002). Administration of rAAV6:HDAC4^{D840N} to denervated muscles, which was readily detected in denervated skeletal muscle, reduced the ensuing muscle atrophy (Fig. S5, b–d). As HDAC4 is a key regulator of myogenin expression in denervated muscles and myogenin plays an indispensible role promoting neurogenic atrophy, we determined that HDAC4^{D840N} also inhibited the expression of myogenin (Fig. S5 e). Significantly, when codelivered with rAAV6:Smad6, HDAC4^{D840N} prevented the exacerbation of muscle atrophy by rAAV6:Smad6, despite sustained Smad6 protein expression and inhibition of Smad1/5 phosphorylation (Fig. 5, d and e). Importantly, whereas rAAV6:Smad6 up-regulated the expression of myogenin in denervated muscles, HDAC4^{D840N} repressed myogenin induction and the subsequent transcription of the E3 ligases MuRF1, atrogin1, and Musa1/Fbxo30 (Fig. 5, f and g). These data demonstrate that in denervated muscles the BMP–Smad1/5 signaling axis is engaged to preserve muscle mass by suppressing the activity of the atrophy-inducing HDAC4–myogenin–E3 ubiquitin ligase axis.

Discussion

Our findings identify a new, essential role of the BMP–Smad1/5/8 axis in the regulation of skeletal muscle mass during growth and wasting. Increasing signaling via the BMP pathway can promote myofiber hypertrophy by stimulating mTOR-dependent anabolic mechanisms. Importantly, the BMP–Smad1/5/8 signaling pathway is vital for conservation of muscle mass after loss of motor nerve activity. As augmentation of BMP signaling can protect muscles from denervation-induced atrophy, the BMP–Smad1/5/8 signaling pathway may represent a new target for the development of therapeutics to ameliorate muscle wasting.

In mature skeletal muscle, activation of the canonical TGF-β signaling pathway—chiefly via myostatin- and activin-promoting phosphorylation of Smad2/3—suppresses protein synthesis and promotes protein catabolism. Our data reveal BMP–Smad1/5/8 signaling as operating counter to the myostatin/activin–Smad2/3 axis, as an important promoter of anabolism and inhibitor of muscle wasting. The stimulation of muscle hypertrophy via increased expression of BMP7 or a constitutively active type-I BMP receptor uses phosphorylation of Smad1/5/8 to activate mTOR-mediated protein synthesis. Inhibition of Smad1/5/8 phosphorylation or mTOR activity prevented BMP-induced muscle hypertrophy and mTOR-mediated anabolic signaling (and in the case of direct mTOR inhibition, despite continued phosphorylation of Smad1/5), thus confirming the mechanism by which BMP receptor stimulation promotes muscle hypertrophy in innervated muscles. These findings contrast with the documented inhibitory effects of the myostatin/activin–Smad2/3 axis upon mTOR-mediated signaling (Trendelenburg et al., 2009; Winbanks et al., 2012). Our findings are consistent with studies of BMP-mediated mTOR activation in other cell types (Langenfeld et al., 2005; Townsend et al., 2012). Interestingly, increased expression of Smad6 had no effect on basal muscle mass and mTOR signaling in the muscles of adult mice. These findings suggest that endogenous levels of Smad1/5/8 phosphorylation do not regulate basal muscle mass, distinct from of the effects of the canonical TGF-β signaling pathway. Specifically, Smad2/3 has been shown to actively repress muscle anabolism, such that activation or inhibition of Smad2/3 promotes atrophy or hypertrophy of skeletal muscle, respectively (Sartori et al., 2009; Winbanks et al., 2012). Collectively, the data indicate the canonical TGF-β signaling pathway uses Smad2/3 as a dominant regulator of basal skeletal muscle mass, whereas the BMP signaling pathway is recruited to promote muscle hypertrophy.

We observed that Smad1/5 phosphorylation is altered in states of muscle growth. During postnatal maturation of muscles in rodents, protein synthesis has been shown to decline markedly from 1 wk of age (Suryawan et al., 2006). In support of a role for the BMP signaling axis associated with the regulation of neonatal muscle development, we demonstrate that Smad1/5 phosphorylation markedly declines in correlation with reported reductions in protein synthesis. In adult musculature, we demonstrated that follistatin-mediated muscle hypertrophy (previously considered a function of Smad2/3 inhibition via antagonism of myostatin and activin) is associated with, and requires, phosphorylation of BMP-regulated Smad proteins to achieve maximal effect. Follistatin may promote Smad1/5/8 phosphorylation by binding and presenting endogenous BMP ligands to their cognate receptor (Amthor et al., 2002). Alternatively, the sequestration of myostatin/activin by follistatin could enable endogenous BMP ligands to engage common receptors for which myostatin and activin have a higher affinity. This hypothesis is consistent with evidence that myostatin can inhibit the phosphorylation of Smad1/5 by preventing receptor engagement by BMP ligands in adipogenic cells (Rebbapragada et al., 2003).

Our studies suggest the BMP–Smad1/5/8 signaling pathway is repressed in muscle by mechanisms dependent on motor nerve activity, as we observed increased Smad1/5 phosphorylation in muscles after motor nerve inactivity, degeneration, and resection. The models in which we observed elevated Smad1/5 phosphorylation mimic muscle wasting associated with intensive care unit–related acute myopathy, amyotrophic lateral sclerosis, and nerve trauma, respectively, which suggests increased BMP signaling is a factor in clinically relevant states of muscle wasting. Seeking to determine why Smad1/5 phosphorylation was increased in denervated muscle, we found that the expression of two BMP ligands, GDF5 and GDF6, and the type-IB BMP receptor, ALK6, were robustly increased after denervation. Interestingly, in other tissues, GDF-5 signaling is highly dependent on ALK6 expression (Nickel et al., 2005). Other BMP ligands such as BMP4 may also potentiate BMP signaling at later time points after denervation. We also observed that

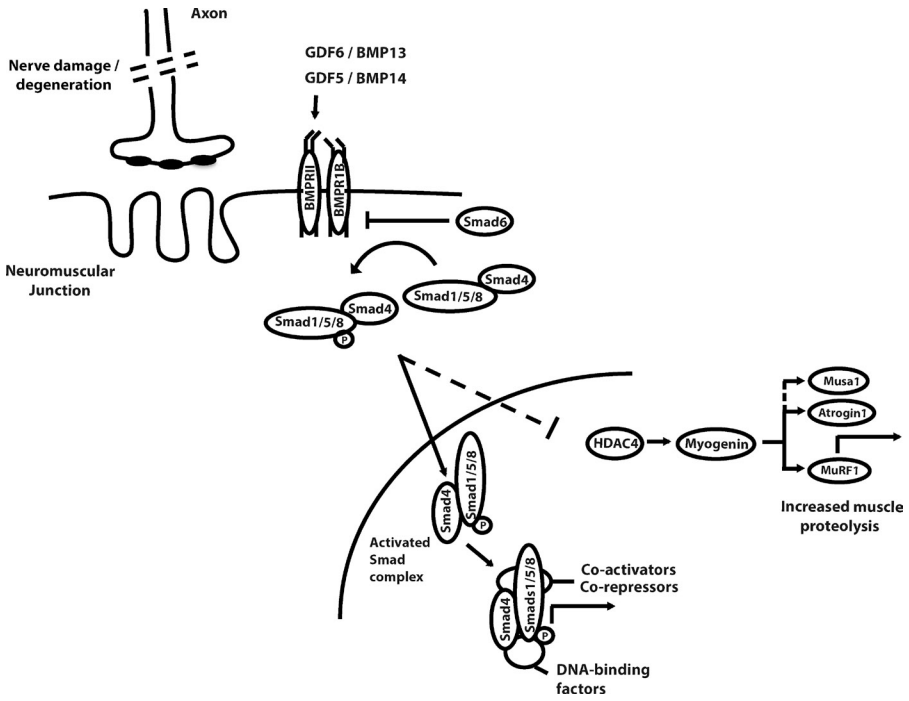

Figure 6. **Proposed schema of how the BMP signaling axis limits neurogenic muscle wasting.** In muscles undergoing neurogenic atrophy, the transcription of BMP ligands GDF5 (BMP14) and GDF6 (BMP13) is increased prominently within skeletal muscle, along with transcription of the type-IB BMP receptor (ALK6) and suppression of the endogenous inhibitor Smad6. The net effect is an increase in Smad1/5/8 phosphorylation. Expression of Smad6 in denervated skeletal muscle exacerbates wasting by suppressing Smad1/5/8 phosphorylation, which in turn potentiates the HDAC4–myogenin pathway, leading to increased transcription of E3 ubiquitin ligases associated with muscle proteolysis, including MuRF1, atrogin1, and Fbxo30/MUSA1.

transcription of the endogenous inhibitory proteins Noggin and Smad6 was repressed in denervated muscles. The coordinated regulation of so many elements within the BMP–Smad1/5/8 axis would account for the increased Smad1/5 phosphorylation observed and indicate that engagement of BMP-mediated signaling plays a significant role in the response of skeletal muscles to perturbation/loss of motor nerve activity (Fig. 6).

We sought to define the functional role of increased BMP signaling in denervated muscles by inhibiting BMP-mediated Smad1/5 phosphorylation, via increased expression of the endogenous inhibitory protein Smad6. Strikingly, we found that increased expression of Smad6 in denervated skeletal muscles exacerbated neurogenic muscle atrophy. These data suggest that BMP signaling is activated in denervated skeletal muscle to protect against neurogenic muscle atrophy. In support of these findings, potentiation of BMP signaling via administration of rAAV6:BMP7 and rAAV6:ALK3 attenuated denervation-induced muscle wasting. We determined that the transcription of specific E3 ubiquitin ligases previously associated with muscle atrophy (MuRF1, atrogin1, and the more recently identified Fbxo30/Musa1) is substantially increased in denervated muscles when BMP–Smad1/5/8 signaling is inhibited (Fig. 6). The transcription of MuRF1 and atrogin1 can be promoted by increased activity of the HDAC–myogenin signaling cascade in muscle, which itself has been implicated as a key driver of neurogenic muscle atrophy (Moresi et al., 2010). Accordingly, we observed that the inhibition of BMP–Smad1/5/8 signaling in denervated muscles markedly potentiated the atrophy-inducing HDAC–myogenin signaling cascade. Critically, as coadministering a dominant-negative HDAC4 with rAAV6:Smad6 to denervated muscles significantly prevented muscle wasting and the induction of myogenin, MuRF1, atrogin1, and Fbxo30/Musa1, our data supports a model whereby BMP signaling suppresses HDAC4–myogenin signaling in denervated muscles to limit neurogenic muscle atrophy (Fig. 6). Although HDAC4^{D840N} did not completely prevent denervation-induced myogenin and E3 ligase induction in the presence of blunted BMP signaling, we hypothesize that this may be a result of functional redundancy between class II HDAC proteins (Potthoff et al., 2007; Moresi et al., 2010). Although it is unclear how the BMP signaling pathway interacts with HDAC proteins, it has been established that BMP-regulated Smad1/5 can repress transcription of myogenin (Katagiri et al., 1997; Yamamoto et al., 1997). In the case of denervated muscles demonstrating increased BMP–Smad1/5/8 signaling, it is therefore possible that phosphorylated Smad1/5 proteins repress both HDACs and myogenin, thereby inhibiting their ability to drive expression of the aforementioned E3 ligases (Fig. 6). As the genetic ablation of the HDACs and myogenin renders muscles resistant to denervation-induced wasting, and the activity of Smad1/5 appears critical for limiting the induction of HDAC–myogenin signaling, our studies suggest there may be considerable potential to ameliorate neurogenic muscle atrophy in clinical conditions using interventions that enhance the BMP–Smad1/5/8 signaling axis in skeletal musculature.

Although our studies have focused on the effect of BMP–Smad1/5 signaling in skeletal muscle, it is intriguing to note that local release of BMP ligands from musculature has been described as critical for supporting nerve terminal development and establishment of the neuromuscular junction (McCabe et al., 2003; Ball et al., 2010). Furthermore, some neuromuscular disorders may be associated with perturbed BMP activity (Pescatori et al., 2007; Bayat et al., 2011). Accordingly, although our data demonstrate that increased expression of specific BMPs in muscle contributes to autocrine BMP-mediated signaling that is vital to limit catabolism in denervated muscles, it is possible that increased BMP expression by denervated muscles may also be stimulated to promote remodeling and/or regeneration of motor

nerve terminals and the neuromuscular junction. Our ongoing research seeks to determine the significance of muscle-derived BMP ligands in developing and maintaining the integral relationship between the motor nerve and muscle fibers in the context of neuromuscular disorders and neurogenic muscle wasting.

In conclusion, we demonstrate for the first time that the BMP signaling axis is a bona fide positive regulator of skeletal muscle mass. This role of BMP–Smad1/5/8 signaling sits in marked contrast to the established negative role of the canonical TGF-β signaling cascade in muscle, which is chiefly considered as the myostatin/activin–Smad2/3 signaling axis. Our studies indicate BMP–Smad1/5/8 signaling is potentiated upon perturbation/loss of motor nerve activity to conserve muscle mass. As our data demonstrate that enhancing BMP signaling is protective in models of neurogenic atrophy, we propose that interventions targeting the BMP–Smad1/5 axis may hold exciting potential as therapeutics capable of ameliorating muscle wasting and should be investigated accordingly.

Materials and methods

Antibodies

All antibodies used were obtained from Cell Signaling Technology, except for antibodies against pSmad3 (Epitomics) and GAPDH (Santa Cruz Biotechnology, Inc.).

Production of rAAV6 vectors

cDNA constructs encoding follistatin-288, Smad6, BMP7, constitutively active ALK3 (GenScript), and $HDAC^{D840N}$ (Fischle et al., 2002) were cloned into an rAAV2 expression plasmid consisting of a CMV promoter/enhancer (with the exception of $HDAC4^{D840N}$ containing a muscle-specific CK6 promoter) and SV40 poly-A region flanked by rAAV2 terminal repeats using standard cloning techniques. Transfection of these plasmids with the pDGM6 packaging plasmid into HEK293 cells generated type-6 pseudotyped viral vectors that were harvested and purified as described previously (Gregorevic et al., 2004). In brief, HEK293 cells were plated at a density of $3.2-3.8 \times 10^6$ cells on 10-cm culture dishes, 8–16 h before transfection with 10 µg of a vector-genome–containing plasmid and 20 µg of the packaging/helper plasmid pDGM6, by means of the calcium phosphate precipitate method to generate pseudotype 6 vectors. 72 h after transfection, the media and cells were collected and homogenized through a microfluidizer (Microfluidics) before 0.22-µm clarification (EMD Millipore). The vector was purified from the clarified lysate by affinity chromatography over a HiTrap heparin column (GE Healthcare) and ultracentrifuged overnight before resuspension in sterile physiological Ringer's solution. The purified vector preparations were titered with a customized sequence-specific quantitative PCR-based reaction (Applied Biosystems).

Animal experiments

All experiments were conducted in accordance with the relevant codes of practice for the care and use of animals for scientific purposes (National Institutes of Health and National Health and Medical Council of Australia). For local vector delivery, mice were deeply anesthetized with isoflurane, and 10^9–2.5×10^{10} vector genomes of a given vector were injected in 30 µl of HBSS directly into the anterior compartment of the hindlimb, which is occupied by the TA and extensor digitorum longus muscles. Control injections of the contralateral limb used a vector lacking a functional gene (referred to as rAAV6:MCS). For rapamycin experiments, rapamycin was dissolved overnight in a solution containing 0.2% carboxymethylcellulose sodium salt (Sigma-Aldrich) and 0.25% polysorbate-80 (Sigma-Aldrich) in water, as described previously (Shioi et al., 2003). In these experiments, 8-wk-old mice received 1 mg/kg/day of rapamycin (EMD Millipore) or vehicle as a daily intraperitoneal injection commencing 3 h before rAAV6:BMP7 injection and continuing for 28 d inclusive. For experiments examining denervation-induced muscle atrophy, 6–8-wk-old mice were deeply anaesthetized and an incision was made laterally below the knee. Here, a 1-mm portion of the peroneal nerve was removed to denervate the TA muscle. While the mouse was under anesthesia, the anterior hindlimb was injected with the appropriate vector, except for rAAV6:BMP7 and rAAV6:ALK3, which were injected 4 wk before denervation. For tissue harvest, mice were humanely killed via cervical dislocation and the muscles were rapidly excised and weighed before subsequent processing. For examination of muscle wasting in a mouse model of amyotrophic lateral sclerosis, transgenic $SOD1^{G93A}$ mice derived from the B6SJL-TgN (SOD1-G93A) 1Gur line (The Jackson Laboratory) were backcrossed onto a pure C57BL/6 background. At the designated time points, $SOD1^{G93A}$ mice and nontransgenic wild-type littermates were killed by lethal injection (100 mg/kg sodium pentobarbitone, intraperitoneally) and the TA muscles were rapidly dissected for processing. For examination of muscle wasting in a rodent model of intensive care unit myopathy, muscle samples were obtained from female Sprague-Dawley rats, representing a subsample generated from a previous study (Ochala et al., 2011). The experimental rats were anaesthetized, treated with the neuromuscular blocker α-cobratoxin, and mechanically ventilated for durations varying from 3 to 13 d. The experimental model has previously been described in detail (Dworkin and Dworkin, 1990; Dworkin and Dworkin, 2004). In brief, the following surgery and instrumentation was completed with sterile technique: (1) Precordial silver wire electrocardiogram electrodes were implanted subcutaneously. (2) An aortic catheter (28-gauge Teflon) was inserted via the left carotid artery to record arterial blood pressure. (3) A 0.9-mm Renathane catheter was threaded into the left jugular vein to administer parental solutions. (4) Three subcutaneous electroencephalography (EEG) needle electrodes were placed into the skull above the right and left temporal lobes, and a third reference electrode was placed in the neck region. (5) Temperature was measured by a vaginal thermistor and servo-regulated at 37°C. (6) A silicone cannula was inserted in the urethra to continuously record urine output. The sham-operated control animals underwent the same interventions as the controls, but they were not pharmacologically paralyzed with α-cobratoxin. That is, sham-operated controls were anesthetized (isoflurane), spontaneously breathing, given intraarterial and i.v. solutions, and killed within 2 h after the initial anesthesia and surgery. During surgery or any possible irritating manipulation, the anesthetic isoflurane level was >1.5%, which maintained the following states: (a) the EEG was synchronized and dominated by high-voltage slow-wave activity; (b) mean arterial pressure was 100 mmHg and the heart rate 420 beats/min; and (c) there were no evident EEG, blood pressure, or heart rate responses to surgical manipulation. Isoflurane was delivered into the inspiratory gas stream by a precision mass-flow controller. After the initial surgery, isoflurane was gradually lowered (over 1 to 2 d) and maintained at <0.5% during the remaining experimental period. Rats were ventilated through a per os coaxial tracheal cannula at 72 breaths/min with an inspiratory and expiratory ratio of 1:2 and a minute volume of 180–200 ml and gas concentrations of 50% O_2, 47% N_2, and 3% CO_2, delivered by a precision volumetric respirator. Intermittent respiratory hyperinflations (6 per hour at 15 cmH_2O), positive end-expiratory pressure (1.5 cmH_2O), and expiratory CO_2 monitoring were continuous. Neuromuscular blockade was induced on the first day (100 µg α-cobratoxin, i.v.) and maintained by continuous infusion (250 µg/d, i.v.). Mechanical ventilation was initiated immediately after the neuromuscular blockade induction. In no case did animals show any signs of infections or septicemia. The ethics committee at Uppsala University approved all aspects of the rodent intensive care unit myopathy study.

Real-time PCR

Total RNA was collected from TA muscles cells using Trizol (Invitrogen). 500–1,000 ng of RNA was reverse transcribed using the High Capacity RNA-to-cDNA kit (Applied Biosystems). Expression levels of all genes analyzed were determined via RT-PCR using Taqman assay on demand kits (Applied Biosystems) and detection software (Applied Biosystems). For detection of BMP7 gene expression, Sybr Green analysis was used (forward: 5′-ggctggcaggactggatcat-3′; reverse: 5′-ggcgcacagcagggcttgg-3′). In all cases, 18S was used to standardize cDNA concentrations. Data were analyzed using the ΔΔCT method of analysis and the control cohort is normalized to a value of 1.

Luciferase experiments

C2C12 cells were either transfected in 24-well plates with 0.35 µg Smad6, ALK3, or BMP7 plasmid and 0.25 µg BRE-*Luc* plasmid or 0.25 µg β-galactosidase expression plasmid per well using lipofectamine 2000 (Invitrogen). Where appropriate, media was changed 16 h later and supplemented with either vehicle or 3 nM BMP4 for 24 h. Cells were then lysed with cell lysis buffer (Promega) and luciferase activity was measured using a Berthold Luminometer. Luciferase activity is presented as the ratio of BRE-luciferase activity to β-galactosidase reporter activity. β-Galactosidase was detected using a β-galactosidase detection assay (Promega). In brief, lysate was incubated with 2× β-galactosidase buffer for 30 min to 1 h at 37°C and expression was then measured at 420 nm.

Histology

Harvested muscles were placed in Optimal Cutting Temperature cryoprotectant (Sakura) and frozen in liquid nitrogen–cooled isopentane. The frozen samples were subsequently cryosectioned at 10-µm thickness and stained with hematoxylin and eosin (H&E) to examine morphology as described previously (Rafael et al., 1996). Sections were mounted using DePeX mounting medium (BDH) and images of stained sections were captured at room temperature using a U-TV1X-2 camera mounted to an IX71 microscope (Olympus) and a PlanC 10×/0.25 objective lens (Olympus). DP2-BSW acquisition software (Olympus) was used to acquire images. Myofiber size and area was determined by placing TA muscles in Optimal Cutting Temperature and freezing in liquid nitrogen–cooled isopentane. The sarcolemma of muscle fibers was then identified using an antibody raised against laminin. In brief, 10-µm sections were fixed in methanol, and then washed in PBS containing 0.2% Tween-20 and subsequently blocked in 5% normal goat serum. Sections were then incubated with rat anti-laminin antibody (EMD Millipore) and a secondary goat anti–rat antibody Alexa 594 (Molecular Probes) was used as the fluorescent label, followed by mounting in Vectashield HardSet (Vector Laboratories). Fluorescent images were taken on a microscope (BX61; Olympus). The minimum Feret's diameter and myofiber area were determined using ImageJ software by measuring at least 600 myofibers per mouse TA muscle and at least three mice were used per group to quantify these variables.

Western blotting

TA muscles were homogenized in RIPA-based lysis buffer (EMD Millipore) with Complete EDTA-free protease and phosphatase inhibitor cocktails (Roche). Lysis was followed by centrifugation at 13,000 *g* for 10 min at 4°C and samples were denatured for 5 min at 95°C. Protein concentration was determined using a Pierce protein assay kit (Thermo Fisher Scientific). Protein fractions were subsequently separated by SDS-PAGE using precast 4–12% Bis-Tris gels (Invitrogen), blotted onto nitrocellulose membranes (Bio-Rad Laboratories), and incubated with the appropriate antibody overnight and detected as described previously (Winbanks et al., 2011). Quantification of labeled Western blots was performed using ImageJ pixel analysis (National Institutes of Health Image software), and data are normalized to a control value of 1. Densitometric analyses of Western blots are presented as band density normalized to the loading control. In cases of phosphorylated proteins, the loading control is the total protein level of that phosphorylated protein. Total protein levels have been quantified by using GAPDH as the loading control.

Statistical analysis

One- or two-way analyses of variance were used to assess statistical differences across multiple conditions, with the Student-Newman-Keuls post-hoc test used for comparisons between the specific group means. Comparisons between two conditions only used the Students' *t* test. Statistics on myofiber diameter were performed on all raw data within a treatment, not on quartile values. Data are reported as statistically significant when $P < 0.05$ for comparisons. Data are presented as the mean ± SEM.

Online supplemental material

Fig. S1 shows that rAAV6:ALK3 can regulate IGF transcription and provides supportive evidence of the ability of rAAV6:BMP7-induced growth to be regulated by mTOR signaling. Fig. S2 demonstrates that Smad6 does not alter basal skeletal muscle mass. Fig. S3 demonstrates the dependency of follistatin-induced muscle growth on BMP signaling in vivo. Fig. S4 illustrates a transcriptional profile of BMP ligands and BMP inhibitors in denervated muscles and also demonstrates that rAAV6:Smad6 does not regulate Foxo and Akt signaling in denervation. Fig. S5 confirms that the administration of rAAV6:HDAC4^{D840N} is protective in denervation-induced muscle wasting. Online supplemental material is available at http://www.jcb.org/cgi/content/full/jcb.201211134/DC1.

The authors thank Graeme Lancaster for his critical feedback on the data in the manuscript.

This work was supported by project grant funding from the National Health and Medical Research Council (NHMRC) of Australia (526648 to P. Gregorevic, 1008910 to B.J. Turner, and 1006488 to C.A. Harrison), a Motor Neuron Disease Research Institute of Australia Mick Rodger Motor Neuron Disease research grant (B.J. Turner), and an initiation grant from the Swedish Foundation for International Cooperation in Research and Higher Education (L. Larsson and P. Gregorevic). C.A. Harrison is supported by a Career Development Fellowship (1013533) from the NHMRC. J.R. McMullen is supported by a Future Fellowship (FT0001657) from the Australian Research Council and an Honorary Senior Research Fellowship (586604) from the NHMRC. S.L. McGee is supported by a Career Development Fellowship (1030474) from the NHMRC. P. Gregorevic is supported by a Career Development Fellowship (1046782) from the NHMRC and, previously, a Senior Research Fellowship sponsored by Pfizer Australia. The Baker IDI Heart and Diabetes Institute is supported in part by the Operational Infrastructure Support Program of the Victorian Government.

The authors declare no conflict of interest.

Author contributions: C.E. Winbanks and P. Gregorevic designed the research. C.E. Winbanks, J.L. Chen, H. Qian, Y. Liu, B.C. Bernardo, C. Beyer, K.I. Watt, R.E. Thomson, T. Connor, B.J. Turner, L. Larsson, and P. Gregorevic performed the experimental work. B.J. Turner, L. Larsson, C.A. Harrison, J.R. McMullen, and S.L. McGee contributed reagents, analytical tools, and technical advice. C.E. Winbanks, B.C. Bernardo, and P. Gregorevic analyzed the data. C.E. Winbanks and P. Gregorevic wrote the manuscript.

Submitted: 26 November 2012
Accepted: 11 September 2013

References

Amthor, H., B. Christ, M. Weil, and K. Patel. 1998. The importance of timing differentiation during limb muscle development. *Curr. Biol.* 8:642–652. http://dx.doi.org/10.1016/S0960-9822(98)70251-9

Amthor, H., B. Christ, F. Rashid-Doubell, C.F. Kemp, E. Lang, and K. Patel. 2002. Follistatin regulates bone morphogenetic protein-7 (BMP-7) activity to stimulate embryonic muscle growth. *Dev. Biol.* 243:115–127. http://dx.doi.org/10.1006/dbio.2001.0555

Ball, R.W., M. Warren-Paquin, K. Tsurudome, E.H. Liao, F. Elazzouzi, C. Cavanagh, B.S. An, T.T. Wang, J.H. White, and A.P. Haghighi. 2010. Retrograde BMP signaling controls synaptic growth at the NMJ by regulating trio expression in motor neurons. *Neuron*. 66:536–549. http://dx.doi.org/10.1016/j.neuron.2010.04.011

Bayat, V., M. Jaiswal, and H.J. Bellen. 2011. The BMP signaling pathway at the *Drosophila* neuromuscular junction and its links to neurodegenerative diseases. *Curr. Opin. Neurobiol.* 21:182–188. http://dx.doi.org/10.1016/j.conb.2010.08.014

Bodine, S.C., E. Latres, S. Baumhueter, V.K. Lai, L. Nunez, B.A. Clarke, W.T. Poueymirou, F.J. Panaro, E. Na, K. Dharmarajan, et al. 2001. Identification of ubiquitin ligases required for skeletal muscle atrophy. *Science*. 294:1704–1708. http://dx.doi.org/10.1126/science.1065874

Bogdanovich, S., T.O. Krag, E.R. Barton, L.D. Morris, L.A. Whittemore, R.S. Ahima, and T.S. Khurana. 2002. Functional improvement of dystrophic muscle by myostatin blockade. *Nature*. 420:418–421. http://dx.doi.org/10.1038/nature01154

Chung, J., C.J. Kuo, G.R. Crabtree, and J. Blenis. 1992. Rapamycin-FKBP specifically blocks growth-dependent activation of and signaling by the 70 kd S6 protein kinases. *Cell*. 69:1227–1236. http://dx.doi.org/10.1016/0092-8674(92)90643-Q

Clever, J.L., Y. Sakai, R.A. Wang, and D.B. Schneider. 2010. Inefficient skeletal muscle repair in inhibitor of differentiation knockout mice suggests a crucial role for BMP signaling during adult muscle regeneration. *Am. J. Physiol. Cell Physiol.* 298:C1087–C1099. http://dx.doi.org/10.1152/ajpcell.00388.2009

Cohen, S., J.J. Brault, S.P. Gygi, D.J. Glass, D.M. Valenzuela, C. Gartner, E. Latres, and A.L. Goldberg. 2009. During muscle atrophy, thick, but not thin, filament components are degraded by MuRF1-dependent ubiquitylation. *J. Cell Biol.* 185:1083–1095. http://dx.doi.org/10.1083/jcb.200901052

Donaldson, C.J., L.S. Mathews, and W.W. Vale. 1992. Molecular cloning and binding properties of the human type II activin receptor. *Biochem. Biophys. Res. Commun.* 184:310–316. http://dx.doi.org/10.1016/0006-291X(92)91194-U

Dworkin, B.R., and S. Dworkin. 1990. Learning of physiological responses: I. Habituation, sensitization, and classical conditioning. *Behav. Neurosci.* 104:298–319. http://dx.doi.org/10.1037/0735-7044.104.2.298

Dworkin, B.R., and S. Dworkin. 2004. Baroreflexes of the rat. III. Open-loop gain and electroencephalographic arousal. *Am. J. Physiol. Regul. Integr. Comp. Physiol.* 286:R597–R605. http://dx.doi.org/10.1152/ajpregu.00469.2003

Fischle, W., F. Dequiedt, M.J. Hendzel, M.G. Guenther, M.A. Lazar, W. Voelter, and E. Verdin. 2002. Enzymatic activity associated with class II HDACs is dependent on a multiprotein complex containing HDAC3 and SMRT/N-CoR. *Mol. Cell*. 9:45–57. http://dx.doi.org/10.1016/S1097-2765(01)00429-4

Gregorevic, P., M.J. Blankinship, J.M. Allen, R.W. Crawford, L. Meuse, D.G. Miller, D.W. Russell, and J.S. Chamberlain. 2004. Systemic delivery of genes to striated muscles using adeno-associated viral vectors. *Nat. Med.* 10:828–834. http://dx.doi.org/10.1038/nm1085

Grönroos, E., I.J. Kingston, A. Ramachandran, R.A. Randall, P. Vizán, and C.S. Hill. 2012. Transforming growth factor β inhibits bone morphogenetic protein-induced transcription through novel phosphorylated Smad1/5-Smad3 complexes. *Mol. Cell. Biol.* 32:2904–2916. http://dx.doi.org/10.1128/MCB.00231-12

Gurney, M.E., H. Pu, A.Y. Chiu, M.C. Dal Canto, C.Y. Polchow, D.D. Alexander, J. Caliendo, A. Hentati, Y.W. Kwon, H.X. Deng, et al. 1994. Motor neuron degeneration in mice that express a human Cu,Zn superoxide dismutase mutation. *Science*. 264:1772–1775. http://dx.doi.org/10.1126/science.8209258

Hayashi, H., S. Abdollah, Y. Qiu, J. Cai, Y.Y. Xu, B.W. Grinnell, M.A. Richardson, J.N. Topper, M.A. Gimbrone Jr., J.L. Wrana, and D. Falb. 1997. The MAD-related protein Smad7 associates with the TGFbeta receptor and functions as an antagonist of TGFbeta signaling. *Cell*. 89:1165–1173. http://dx.doi.org/10.1016/S0092-8674(00)80303-7

Heitman, J., N.R. Movva, and M.N. Hall. 1991. Targets for cell cycle arrest by the immunosuppressant rapamycin in yeast. *Science*. 253:905–909. http://dx.doi.org/10.1126/science.1715094

Holley, S.A., J.L. Neul, L. Attisano, J.L. Wrana, Y. Sasai, M.B. O'Connor, E.M. De Robertis, and E.L. Ferguson. 1996. The *Xenopus* dorsalizing factor noggin ventralizes *Drosophila* embryos by preventing DPP from activating its receptor. *Cell*. 86:607–617. http://dx.doi.org/10.1016/S0092-8674(00)80134-8

Ibebunjo, C., J.M. Chick, T. Kendall, J.K. Eash, C. Li, Y. Zhang, C. Vickers, Z. Wu, B.A. Clarke, J. Shi, et al. 2013. Genomic and proteomic profiling reveals reduced mitochondrial function and disruption of the neuromuscular junction driving rat sarcopenia. *Mol. Cell. Biol.* 33:194–212. http://dx.doi.org/10.1128/MCB.01036-12

Imamura, T., M. Takase, A. Nishihara, E. Oeda, J. Hanai, M. Kawabata, and K. Miyazono. 1997. Smad6 inhibits signalling by the TGF-beta superfamily. *Nature*. 389:622–626. http://dx.doi.org/10.1038/39355

Ishida, W., T. Hamamoto, K. Kusanagi, K. Yagi, M. Kawabata, K. Takehara, T.K. Sampath, M. Kato, and K. Miyazono. 2000. Smad6 is a Smad1/5-induced smad inhibitor. Characterization of bone morphogenetic protein-responsive element in the mouse Smad6 promoter. *J. Biol. Chem.* 275:6075–6079. http://dx.doi.org/10.1074/jbc.275.9.6075

Kalista, S., O. Schakman, H. Gilson, P. Lause, B. Demeulder, L. Bertrand, M. Pende, and J.P. Thissen. 2012. The type 1 insulin-like growth factor receptor (IGF-IR) pathway is mandatory for the follistatin-induced skeletal muscle hypertrophy. *Endocrinology*. 153:241–253. http://dx.doi.org/10.1210/en.2011-1687

Kambadur, R., M. Sharma, T.P. Smith, and J.J. Bass. 1997. Mutations in myostatin (GDF8) in double-muscled Belgian Blue and Piedmontese cattle. *Genome Res.* 7:910–916.

Katagiri, T., S. Akiyama, M. Namiki, M. Komaki, A. Yamaguchi, V. Rosen, J.M. Wozney, A. Fujisawa-Sehara, and T. Suda. 1997. Bone morphogenetic protein-2 inhibits terminal differentiation of myogenic cells by suppressing the transcriptional activity of MyoD and myogenin. *Exp. Cell Res.* 230:342–351. http://dx.doi.org/10.1006/excr.1996.3432

Langenfeld, E.M., Y. Kong, and J. Langenfeld. 2005. Bone morphogenetic protein-2-induced transformation involves the activation of mammalian target of rapamycin. *Mol. Cancer Res.* 3:679–684. http://dx.doi.org/10.1158/1541-7786.MCR-05-0124

Latres, E., A.R. Amini, A.A. Amini, J. Griffiths, F.J. Martin, Y. Wei, H.C. Lin, G.D. Yancopoulos, and D.J. Glass. 2005. Insulin-like growth factor-1 (IGF-1) inversely regulates atrophy-induced genes via the phosphatidylinositol 3-kinase/Akt/mammalian target of rapamycin (PI3K/Akt/mTOR) pathway. *J. Biol. Chem.* 280:2737–2744. http://dx.doi.org/10.1074/jbc.M407517200

Lee, S.J. 2007. Quadrupling muscle mass in mice by targeting TGF-beta signaling pathways. *PLoS ONE*. 2:e789. http://dx.doi.org/10.1371/journal.pone.0000789

Lee, S.J., and A.C. McPherron. 2001. Regulation of myostatin activity and muscle growth. *Proc. Natl. Acad. Sci. USA*. 98:9306–9311. http://dx.doi.org/10.1073/pnas.151270098

Lee, S.J., Y.S. Lee, T.A. Zimmers, A. Soleimani, M.M. Matzuk, K. Tsuchida, R.D. Cohn, and E.R. Barton. 2010. Regulation of muscle mass by follistatin and activins. *Mol. Endocrinol.* 24:1998–2008. http://dx.doi.org/10.1210/me.2010-0127

Massagué, J., J. Seoane, and D. Wotton. 2005. Smad transcription factors. *Genes Dev.* 19:2783–2810. http://dx.doi.org/10.1101/gad.1350705

Mathews, L.S., W.W. Vale, and C.R. Kintner. 1992. Cloning of a second type of activin receptor and functional characterization in *Xenopus* embryos. *Science*. 255:1702–1705. http://dx.doi.org/10.1126/science.1313188

McCabe, B.D., G. Marqués, A.P. Haghighi, R.D. Fetter, M.L. Crotty, T.E. Haerry, C.S. Goodman, and M.B. O'Connor. 2003. The BMP homolog Gbb provides a retrograde signal that regulates synaptic growth at the *Drosophila* neuromuscular junction. *Neuron*. 39:241–254. http://dx.doi.org/10.1016/S0896-6273(03)00426-4

McPherron, A.C., A.M. Lawler, and S.J. Lee. 1997. Regulation of skeletal muscle mass in mice by a new TGF-beta superfamily member. *Nature*. 387:83–90. http://dx.doi.org/10.1038/387083a0

Moresi, V., A.H. Williams, E. Meadows, J.M. Flynn, M.J. Potthoff, J. McAnally, J.M. Shelton, J. Backs, W.H. Klein, J.A. Richardson, et al. 2010. Myogenin and class II HDACs control neurogenic muscle atrophy by inducing E3 ubiquitin ligases. *Cell*. 143:35–45. http://dx.doi.org/10.1016/j.cell.2010.09.004

Musarò, A., K.J. McCullagh, F.J. Naya, E.N. Olson, and N. Rosenthal. 1999. IGF-1 induces skeletal myocyte hypertrophy through calcineurin in association with GATA-2 and NF-ATc1. *Nature*. 400:581–585. http://dx.doi.org/10.1038/23060

Nakao, A., M. Afrakhte, A. Morén, T. Nakayama, J.L. Christian, R. Heuchel, S. Itoh, M. Kawabata, N.E. Heldin, C.H. Heldin, and P. ten Dijke. 1997. Identification of Smad7, a TGFbeta-inducible antagonist of TGF-beta signalling. *Nature*. 389:631–635. http://dx.doi.org/10.1038/39369

Nickel, J., A. Kotzsch, W. Sebald, and T.D. Mueller. 2005. A single residue of GDF-5 defines binding specificity to BMP receptor IB. *J. Mol. Biol.* 349:933–947. http://dx.doi.org/10.1016/j.jmb.2005.04.015

Ochala, J., A.M. Gustafson, M.L. Diez, G. Renaud, M. Li, S. Aare, R. Qaisar, V.C. Banduseela, Y. Hedström, X. Tang, et al. 2011. Preferential skeletal muscle myosin loss in response to mechanical silencing in a novel rat intensive care unit model: underlying mechanisms. *J. Physiol.* 589:2007–2026. http://dx.doi.org/10.1113/jphysiol.2010.202044

Pescatori, M., A. Broccolini, C. Minetti, E. Bertini, C. Bruno, A. D'amico, C. Bernardini, M. Mirabella, G. Silvestri, V. Giglio, et al. 2007. Gene expression profiling in the early phases of DMD: a constant molecular signature characterizes DMD muscle from early postnatal life throughout disease progression. *FASEB J.* 21:1210–1226. http://dx.doi.org/10.1096/fj.06-7285com

Potthoff, M.J., H. Wu, M.A. Arnold, J.M. Shelton, J. Backs, J. McAnally, J.A. Richardson, R. Bassel-Duby, and E.N. Olson. 2007. Histone deacetylase degradation and MEF2 activation promote the formation of slow-twitch myofibers. *J. Clin. Invest.* 117:2459–2467. http://dx.doi.org/10.1172/JCI31960

Pourquié, O., C.M. Fan, M. Coltey, E. Hirsinger, Y. Watanabe, C. Bréant, P. Francis-West, P. Brickell, M. Tessier-Lavigne, and N.M. Le Douarin. 1996. Lateral and axial signals involved in avian somite patterning: a role for BMP4. *Cell*. 84:461–471. http://dx.doi.org/10.1016/S0092-8674(00)81291-X

Rafael, J.A., G.A. Cox, K. Corrado, D. Jung, K.P. Campbell, and J.S. Chamberlain. 1996. Forced expression of dystrophin deletion constructs reveals structure-function correlations. *J. Cell Biol.* 134:93–102. http://dx.doi.org/10.1083/jcb.134.1.93

Rebbapragada, A., H. Benchabane, J.L. Wrana, A.J. Celeste, and L. Attisano. 2003. Myostatin signals through a transforming growth factor beta-like signaling pathway to block adipogenesis. *Mol. Cell. Biol.* 23:7230–7242. http://dx.doi.org/10.1128/MCB.23.20.7230-7242.2003

Rommel, C., S.C. Bodine, B.A. Clarke, R. Rossman, L. Nunez, T.N. Stitt, G.D. Yancopoulos, and D.J. Glass. 2001. Mediation of IGF-1-induced skeletal myotube hypertrophy by PI(3)K/Akt/mTOR and PI(3)K/Akt/GSK3 pathways. *Nat. Cell Biol.* 3:1009–1013. http://dx.doi.org/10.1038/ncb1101-1009

Ruschke, K., C. Hiepen, J. Becker, and P. Knaus. 2012. BMPs are mediators in tissue crosstalk of the regenerating musculoskeletal system. *Cell Tissue Res.* 347:521–544. http://dx.doi.org/10.1007/s00441-011-1283-6

Sako, D., A.V. Grinberg, J. Liu, M.V. Davies, R. Castonguay, S. Maniatis, A.J. Andreucci, E.G. Pobre, K.N. Tomkinson, T.E. Monnell, et al. 2010. Characterization of the ligand binding functionality of the extracellular domain of activin receptor type IIb. *J. Biol. Chem.* 285:21037–21048. http://dx.doi.org/10.1074/jbc.M110.114959

Sandri, M., C. Sandri, A. Gilbert, C. Skurk, E. Calabria, A. Picard, K. Walsh, S. Schiaffino, S.H. Lecker, and A.L. Goldberg. 2004. Foxo transcription factors induce the atrophy-related ubiquitin ligase atrogin-1 and cause skeletal muscle atrophy. *Cell*. 117:399–412. http://dx.doi.org/10.1016/S0092-8674(04)00400-3

Sartori, R., G. Milan, M. Patron, C. Mammucari, B. Blaauw, R. Abraham, and M. Sandri. 2009. Smad2 and 3 transcription factors control muscle mass in adulthood. *Am. J. Physiol. Cell Physiol.* 296:C1248–C1257. http://dx.doi.org/10.1152/ajpcell.00104.2009

Sartori, R., E. Schirwis, B. Blaauw, S. Bortolanza, E. Enzo, A. Stantzou, E. Mouisel, L. Toniolo, A. Ferry, S. Stricker, et al. 2013. BMP signaling controls muscle mass. *Nat. Genet.* http://dx.doi.org/10.1038/ng.2772

Shioi, T., J.R. McMullen, O. Tarnavski, K. Converso, M.C. Sherwood, W.J. Manning, and S. Izumo. 2003. Rapamycin attenuates load-induced cardiac hypertrophy in mice. *Circulation*. 107:1664–1670. http://dx.doi.org/10.1161/01.CIR.0000057979.36322.88

Stitt, T.N., D. Drujan, B.A. Clarke, F. Panaro, Y. Timofeyva, W.O. Kline, M. Gonzalez, G.D. Yancopoulos, and D.J. Glass. 2004. The IGF-1/PI3K/Akt

pathway prevents expression of muscle atrophy-induced ubiquitin ligases by inhibiting FOXO transcription factors. *Mol. Cell*. 14:395–403. http://dx.doi.org/10.1016/S1097-2765(04)00211-4

Suryawan, A., J.W. Frank, H.V. Nguyen, and T.A. Davis. 2006. Expression of the TGF-beta family of ligands is developmentally regulated in skeletal muscle of neonatal rats. *Pediatr. Res.* 59:175–179. http://dx.doi.org/10.1203/01.pdr.0000196718.47935.6e

Tang, H., P. Macpherson, M. Marvin, E. Meadows, W.H. Klein, X.J. Yang, and D. Goldman. 2009. A histone deacetylase 4/myogenin positive feedback loop coordinates denervation-dependent gene induction and suppression. *Mol. Biol. Cell*. 20:1120–1131. http://dx.doi.org/10.1091/mbc.E08-07-0759

Townsend, K.L., R. Suzuki, T.L. Huang, E. Jing, T.J. Schulz, K. Lee, C.M. Taniguchi, D.O. Espinoza, L.E. McDougall, H. Zhang, et al. 2012. Bone morphogenetic protein 7 (BMP7) reverses obesity and regulates appetite through a central mTOR pathway. *FASEB J.* 26:2187–2196. http://dx.doi.org/10.1096/fj.11-199067

Trendelenburg, A.U., A. Meyer, D. Rohner, J. Boyle, S. Hatakeyama, and D.J. Glass. 2009. Myostatin reduces Akt/TORC1/p70S6K signaling, inhibiting myoblast differentiation and myotube size. *Am. J. Physiol. Cell Physiol.* 296:C1258–C1270. http://dx.doi.org/10.1152/ajpcell.00105.2009

Winbanks, C.E., B. Wang, C. Beyer, P. Koh, L. White, P. Kantharidis, and P. Gregorevic. 2011. TGF-beta regulates miR-206 and miR-29 to control myogenic differentiation through regulation of HDAC4. *J. Biol. Chem.* 286:13805–13814. http://dx.doi.org/10.1074/jbc.M110.192625

Winbanks, C.E., K.L. Weeks, R.E. Thomson, P.V. Sepulveda, C. Beyer, H. Qian, J.L. Chen, J.M. Allen, G.I. Lancaster, M.A. Febbraio, et al. 2012. Follistatin-mediated skeletal muscle hypertrophy is regulated by Smad3 and mTOR independently of myostatin. *J. Cell Biol.* 197:997–1008. http://dx.doi.org/10.1083/jcb.201109091

Yamamoto, N., S. Akiyama, T. Katagiri, M. Namiki, T. Kurokawa, and T. Suda. 1997. Smad1 and smad5 act downstream of intracellular signalings of BMP-2 that inhibits myogenic differentiation and induces osteoblast differentiation in C2C12 myoblasts. *Biochem. Biophys. Res. Commun.* 238:574–580. http://dx.doi.org/10.1006/bbrc.1997.7325

Zhou, X., J.L. Wang, J. Lu, Y. Song, K.S. Kwak, Q. Jiao, R. Rosenfeld, Q. Chen, T. Boone, W.S. Simonet, et al. 2010. Reversal of cancer cachexia and muscle wasting by ActRIIB antagonism leads to prolonged survival. *Cell*. 142:531–543. http://dx.doi.org/10.1016/j.cell.2010.07.011

Zimmerman, L.B., J.M. De Jesús-Escobar, and R.M. Harland. 1996. The Spemann organizer signal noggin binds and inactivates bone morphogenetic protein 4. *Cell*. 86:599–606. http://dx.doi.org/10.1016/S0092-8674(00)80133-6